Article

Journal of the Brazilian Chemical Society

https://dx.doi.org/10.21577/0103-5053.20240216

*J. Braz. Chem. Soc.* **2025**, *36*, 5, e-20240216, 1-16


# Computational and Experimental Study of PVA with F127 and Citric Acid for Electrospinning

*Ariane Regina S. Rossin,[a,b] Vinicius Martinelli,[a] Ernani A. Basso,[a] Mariana S. Gibin,[c] Vitor S. Zanuto,[c] Bruno Henrique Vilsinski,[d] Eduardo Radovanovic,[a] Wilker Caetano[a] and Douglas C. Dragunski*[a,b]

[a]Grupo Interdisciplinar de Fotoquímica e Eletroquímica Ambiental, Centro de Engenharias e Ciências Exatas, Universidade Estadual do Oeste do Paraná, 85903-000 Toledo-PR, Brazil

[b]Departamento de Química, Universidade Estadual de Maringá, 87020-900 Maringá-PR, Brazil

[c]Departamento de Física, Universidade Estadual de Maringá, 87020-900 Maringá-PR, Brazil

[d]Grupo de Materiais Biopoliméricos e Compósitos (GMBC), Universidade Federal de Juiz de Fora, 36036-900 Juiz de Fora-MG, Brazil

Despite the widespread application of electrospun membranes across various scientific fields, there remains a need for a deeper understanding of the molecular interactions between polymers and other compounds in precursor solutions for electrospinning. This study evaluates the molecular conformations of poly(vinyl alcohol) (PVA) with different degrees of hydrolysis ($PVA_{87}$ and $PVA_{99}$) and high molar mass, crosslinked with citric acid (CA), using molecular modeling. The solution properties, including rheology and conductivity, were compared to obtain electrospun nanofibers. Additionally, Pluronic-F127® (F127) was incorporated into the PVA/CA system for advanced applications. The molecular modeling results indicate that the degree of hydrolysis affects the intermolecular forces of PVA and the effective binding of CA to the polymer chain. The interactions within the PVA/CA/F127 system vary with the degree of hydrolysis. The high viscosity of $PVA_{99}$, due to inter- and intramolecular bonds, negatively impacts fiber morphology and formation. Thermal and Raman analyses confirmed crosslinking. Under the conditions used, the $PVA_{99}$/CA/F127 system is unsuitable for electrospinning. In contrast, the electrospinning and crosslinking of $PVA_{87}$/CA/F127 with high molar mass yielded better results, enhancing the potential of these nanofibers for drug delivery applications.

**Keywords:** polymer rheology, NCI isosurface, materials development, electrospun matrixes

## Introduction

Polymeric fibers are very versatile materials and have had evidence since prehistory. The first manufactured fiber was nylon fiber, which was widely used and propelled more scientists to discover new types of raw material to be spun.[1] Electrospinning is currently well known for forming nanoscale fibers and nanostructured materials in a versatile and intelligent way.[2] It is a simple and promising technique, being possible to be performed in any laboratory requiring a high voltage source, infusion pump, capillary coupled to a syringe, and a metal collector.[3]

To obtain control over the electrospun fibers, the potential of electrospinning can be explored more deeply. Solution parameters, processing conditions, and environmental conditions can be widely varied, chosen, and manipulated to formulate improved nanofiber characteristics.[4] The properties of the solution are predominant factors in excellent electrospinning and, consequently, in the morphology of the fibers. The molecular weight of the polymer, the entanglement of the polymer chains in the solution, and the surface tension are responsible for maintaining the continuous jet in the electrospinning.[5] Further understanding of these parameters can provide progress in obtaining these fibers.[6]

The union of the experimental part with the computational part for electrospinning systems is a reality, and molecular

*e-mail: dcdragunski@gmail.com
Editor handled this article: Fernando C. Giacomelli (Associate)

modeling can be highlighted. Molecular modeling (MM) can be a valuable tool for electrospinning as it can help improve parameter performance that is not explainable experimentally in more depth.[7] It assists in understanding polymer chain behavior, intermolecular forces, viscosity, and surface tension.[8] Lu *et al*.[9] used MM to evaluate the orientation energy of the ethylene/vinyl alcohol copolymer molecule in different solvents and how this factor affects electrospinning. Vao-soongnern *et al*.[10] used MM to see the effect of molecular weight and the conformation of the polymer chain of poly(ethylene oxide) in the properties of electrospun nanofibers.

Here, we describe for the first time, the molecular modeling of a poly(vinyl alcohol) (PVA) solution for electrospinning. PVA is a synthetic polymer obtained from the partial or complete hydrolysis of poly(vinyl acetate) (PVAc), with its first synthesis dating in 1924 by Hermann and Haehnel.[11] During the first half of the 20$^{th}$ century, it was one of the most widely used synthetic polymers in industry sectors, such as trade, medicine, and food, due to its low environmental impact.[12,13] The chemical and physical properties of PVA can vary according to the degree of hydrolysis (DH) (70-100%) and polymerization (10 to 190 KDa), leading to different molecular weights, solubility, particularity, flexibility, solvation, among others.[13,14]

One of the difficulties in applying PVA in electrospinning is its solubility in water; therefore, its crosslinking is necessary for stabilization in humid conditions.[15] Several methodologies for PVA crosslinking, whether chemical or physical, are found in the literature. When comparing the crosslinking types, chemistry shows lower energy and time consumption advantages and improves morphological and biomechanical characteristics.[16] Among the crosslinkers discussed in the literature, citric acid (CA) has been widely used because it is considered a green crosslinker, non-toxic, biocompatible, inexpensive, and can help in the adhesion and proliferation of cells.[17]

Crosslinking of PVA with CA can occur by heat treatment (range 80 to 150 °C) or microwave irradiation.[18] Crosslinking occurs with an esterification reaction between the hydroxyl (OH) groups of PVA and the carboxylic groups of CA. Temperature is applied to activate the esterification and formation of CA anhydride.[19] Nataraj *et al*.[20] have already reported satisfactory results in crosslinking electrospun membranes made of PVA with CA and the stability of the fibers after 72 h of immersion in water. Fraga *et al*.[21] reported the crosslinking of electrospun PVA membranes with high molar mass and degree of hydrolysis with CA (3% m/v) and their stability in water as well.

Still, aiming at more advanced applications, the insertion of Pluronic® F-127 (F127) for possible drug delivery was also studied. F127 are block copolymers composed of basic units of poly(ethylene oxide) (PEO) and poly(propylene oxide) (PPO) forming a PEO-PPO-PEO structure, the PEO units are more hydrophilic, while the PPO units are more hydrophobic. Thus, in an aqueous medium, F127 tends to self-assemble into micelles, forming a support network for the active drug.[22] It has shown promising results when applied in drug delivery systems providing improvements in biopharmaceutical, pharmacodynamic and pharmacokinetic properties.[23] The electrospinning of PVA/F127 solutions has not yet been widely studied. Among the few reports, such as that of El-Aassar *et al*.,[24] indicate that the material has a promising approach for the treatment of wounds, skin infections, and tissue regeneration. For PVA/F127/CA, no studies were found in the literature that address the characteristics of the solution or electrospinning.

In this study, we describe in an unprecedented way the use of molecular modeling to observe the behavior of the PVA solution in different degrees of hydrolysis crosslinked with CA; with the addition of F127. The conformational structure of the molecules was simulated in a solvent. The rheological, and conductivity studies were used to prove the solution parameters. We also evaluated morphological, structural, and thermal properties. For the first time, the structural conformation of PVA under different degrees of hydrolysis, PVA/CA, and PVA/CA/F127 simulated in solution is reported. Additionally, the structure of PVA containing a large amount of mers (n = 17) together with CA and F127 has never been explored. The use of molecular modeling and electrospinning is still poorly explored. Therefore, this original work seeks a more robust approach between theoretical chemistry and electrospinning.

## Experimental

### Materials

$PVA_{99}$ (molecular weight (Mw) 146.000-186.000 g mol$^{-1}$, 99+% hydrolyzed), $PVA_{87}$ (Mw 146.000-186.000, 87-89% hydrolyzed), Pluronic® F127 (Mw = 12.600 g mol$^{-1}$) and citric acid (Mw = 192.12 g mol$^{-1}$, ≥ 99.5%) were acquired from Sigma-Aldrich (São Paulo, Brazil). Ethanol (EtOH; 99.8%) and acetic acid (AAce; 99.8%) were obtained from Synth solvents (Diadema, Brazil).

### Preparation of the solution for electrospinning

The initial solution was prepared from the mass of PVA fixed at 8% m/v with DH of > 99% and 87-88% solubilized in distilled water, using a bath with continuous stirring at 80 °C

for approximately 8 h. After dissolution and cooling, masses of 5 and 10% (m/v) CA crosslinker relative to polymer mass were added to the solution and left under stirring at room temperature for 2 h (step I, Figure 1). Subsequently, thin films of 1% (m/v) of F127 were prepared following the methodology proposed by da Silva *et al.*[25] For this, F127 was dissolved in ethanol and rotary evaporated at 50 °C until a solid F127 film formed and left in a desiccator for 24 h (step II, Figure 1). Finally, the aqueous PVA/CA solution was poured onto the F127 (step III, Figure 1) film and stirred in a bath at 40 °C until complete miscibility.

## Electrospun parameters

The PVA solution was spun from optimal conditions already reported by Rwei and Huang.[26] The PVA/F127/CA solution was placed in a plastic syringe and connected to a metal needle with a straight tip. Wiring parameters were used: voltage of 20 kV, flow of 1 mL $h^{-1}$, distance between the collector of 15 cm, needle diameter of 0.8 × 25 mm, collection system with rotation of 325 cm $s^{-1}$, ambient temperature of 26 ± 4 °C, and relative humidity of 30%. The fibers were deposited in an aluminum foil covered over the collector. At the end of the process, the electrospun matrices were placed on glass plates and taken to the air oven at 110 °C for the crosslinking reaction.[27] The membranes were designated according to the composition of the solution, as shown in Table 1.

**Table 1.** Composition of electrospun membranes

| Electrospun membrane | DH / % | PVA / % (m/v) | F127 / % (m/v) | CA[a] / % (m/v) |
|---|---|---|---|---|
| $PVA_{87}$ | 87-88 | 8 | – | – |
| $PVA_{99}$ | > 99 | 8 | – | – |
| $PVA_{87}/F127/CA_5$ | 87-88 | 8 | 1 | 5 |
| $PVA_{87}/F127/CA_{10}$ | 87-88 | 8 | 1 | 10 |
| $PVA_{99}/F127/CA_5$ | > 99 | 8 | 1 | 5 |
| $PVA_{99}/F127/CA_{10}$ | > 99 | 8 | 1 | 10 |

[a]Relative to polymer mass. DH: degree of hydrolysis; PVA: poly(vinyl alcohol); CA: citric acid.

## Molecular modeling

Computational studies started with the structural optimization of $PVA_{87}$, $PVA_{99}$, CA, and F127. Then, CA interactions with $PVA_{87}$ and $PVA_{99}$ were performed, and the interaction of F127 with the CA-$PVA_{87}$ and CA-$PVA_{99}$ complexes ended. All structures were designed in Avogadro software[28] and optimized in ORCA 5.0 software[29] using the theory level Extended Tight-Binding version 2 (XTB2).[30] Then, single-point calculations were performed with the theory level Perdew-Burke-Ernzerhof (PBE)/Def2 Triple-Zeta Valence with Double Polarization Functions Def2-TZVPP[31,32] considering the D3(Becke-Johnson (BJ)) empirical dispersion correction method.[33] The solvation effect of water was assessed using the Solvent Model Density (SMD) implicit method.[34]

The $PVA_{87}$ and $PVA_{99}$ fragments contain 17 polymeric mers. For its construction, a rectilinear orientation of the mers was considered, and the position of the hydroxyls was varied for $PVA_{99}$ and hydroxyl and acetate groups for $PVA_{87}$. Then, obtaining the optimized fragments in XTB2, two polymeric fragments were complexed in various orientations, and the complexation energy ($\Delta E_{comp}$) was calculated with equation 1:

$$\Delta E_{comp} = E_{2PVA} - 2E_{PVA} \quad (1)$$

where $E_{2PVA}$ is the energy of the complex with two PVA fragments and $E_{PVA}$ the energy of a single fragment determined with a single point in PBE/Def2-TZVPP/SMD (water).

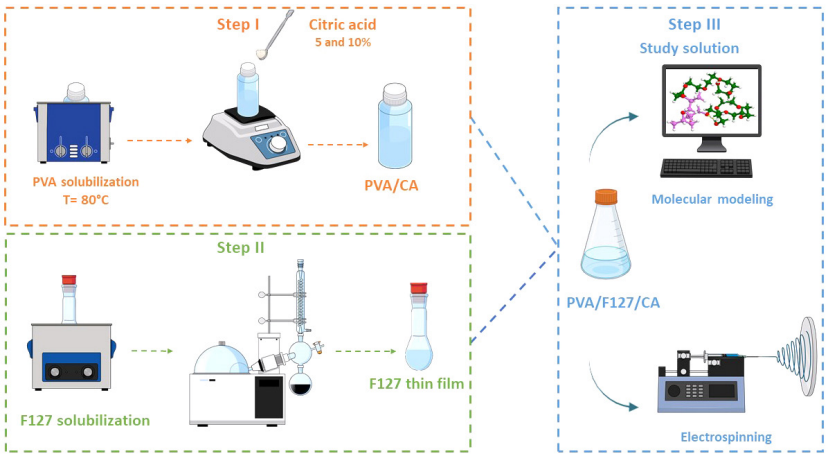


**Figure 1.** Illustrative representation of the preparation of the working solution.

The structures with the highest $\Delta E_{comp}$ were then added. The ABCluster software[35,36] was used for this, which uses the Artificial Bee Colony algorithm to generate complexes systematically. Initially, 50 interaction structures of the CA with the PVA complexes (CA-PVA) were developed, optimized in XTB2, and subsequently submitted to single-point calculations in PBE/Def2-TZVPP//SMD (water). The CA interaction energy with the 2 PVA fragments was calculated using equation 2.

$$\Delta E_{comp} = E_{2PVA/CA} - E_{2PVA} - E_{CA} \quad (2)$$

where $E_{2PVA/CA}$ is the energy of the complex with two PVA fragments with the addition of CA and $E_{CA}$ the energy of the isolated CA.

From the structures with the largest $\Delta E_{comp}$, F127 was added using the same protocol previously mentioned for the addition of CA. In this case, due to the size of the structures and high computational cost, single-point calculations were performed in PBE/Def2-SVP//SMD (water). The interaction energy of F127 was calculated with equation 3.

$$\Delta E_{comp} = E_{F127/2PVA/CA} - E_{2PVA/CA} - E_{F127} \quad (3)$$

where $E_{F127/2PVA/CA}$ is complex energy with two fragments of PVA, CA, and F127 and $E_{F127}$ the energy of F127 isolated.

The equations 1, 2 and 3 are used to describe the energy variation upon interaction between molecules, or in this case, the fragments. The second and third terms on the right side consider the energy of a system where both fragments are infinitely separated, in another word, there is no interaction between them. The first term on the right side considers a system where both fragments are located in the optimal position to minimize the total electronic energy, indicating that they are interacting. The difference between the system where the fragments are infinitely separated (second and third term on the right side) and the system where fragments are interacting (first term on the right side) reflects the energy change resulting from the interaction.

Non-Covalent Interactions (NCI) analyses were performed using the NCIPLOT software[37] using the promolecular approximation.

### Solutions characterizations

The conductivity of the solutions was evaluated using a MS TECNOPON (Piracicaba, Brazil) conductivity meter, model mCE-105, with a measurement range of 0 to 200 mS $cm^{-1}$, cell constant (C) of 1 ± 0.2, resolution of 0.1 µS $cm^{-1}$, and electrode area of 140 mm × (diameter) 10 mm. The temperature of the measurement solutions was 25 ± 3 °C. The electrode was immersed in the previously prepared solutions and left in contact until stabilization, and the data were recorded.

The rheological analysis was performed with continuous shear using a gradient rheometer and controlled shear stress MARS II (Haake®) (Karlsruhe, Germany) at room temperature, with 35 mm cone-plate geometry. The solutions were carefully poured onto the lower plate of the equipment and allowed to rest for 2 min before each reading. The ascending and descending flow curves were obtained with a shear gradient from 0 to 2000 $s^{-1}$. The shear gradient was increased throughout 150 s. The ascending descending curves were analyzed using the Ostwald de Waele (Power Law) equation (equation 4) to obtain the K and n indices.

$$\tau = K\gamma^n \quad (4)$$

where τ = shear stress, K = consistency index; n = flow behavior index; γ = shear rate.

The Casson and Herschel-Buckley rheological models were used to obtain the yield value and are presented in equations 5 and 6.

$$\tau = \sqrt[n]{(\tau_0^n + (\gamma\eta_p))^n} \quad (5)$$

where τ = shear stress, n = flow index, $\tau_0$ = yield value, γ = shear gradient, $\eta_p$ = Casson plastic viscosity.

$$\tau = \tau_0 + k\gamma^n \quad (6)$$

where: τ = shear stress, $\tau_0$ = yield value, k = consistency index, γ = shear gradient, n = flow index.

In addition, the area of thixotropy (At) was obtained using the RheoWin 4.10.0000[38] program (Haake®).

### Characterization of membranes electrospun

The surface morphology of the polymer matrices was evaluated by scanning electron microscopy. The equipment used was a FEI QUANTA series 250 line (Massachusetts, USA). To make the samples electrically conductive, they were deposited on double-sided carbon adhesive tape and metalized with gold to a thickness of 30 nm. The images were obtained by applying an electron-accelerating voltage ranging from 12 to 20 kV at different magnifications. Scanning electron microscope (SEM) images were used to determine mean fiber diameter using ImageJ[39] image processing software, performing measurements on random parts of random fibers (n = 100). Results are expressed as mean ± standard deviation (SD).

Structural and chemical information was verified by Micro-Raman microscopy. The equipment used was a Micro-Raman model Senterra by Bruker, (Massachusetts, USA) with a laser at 785 nm, power of 100 mW, integration time of 5 s, and resolution of 9-15 $cm^{-1}$.

The thermogravimetric analysis technique was used to verify the thermal stability of the electrospun matrices. Data were registered in a PerkinElmer STA 6000 (Waltham, USA) equipment with a ceramic note containing 5 to 10 mg samples. The experiment was conducted in a nitrogen atmosphere with a 50 mL $min^{-1}$ heating rate of 10 °C $min^{-1}$ flow in the temperature range from 30 to 550 °C.

To confirm the crosslinking of the materials, stability in aqueous media was used. For this, the electrospun and cross-linked membranes with CA measuring 1 × 1 $cm^2$ were immersed in distilled water for 24 h. After the time had elapsed, the material was freeze-dried for 24 h using EDWARDS (Cleveland, USA) freeze-drying equipment. Stability in aqueous media was evaluated using a scanning SEM.

## Results and Discussion

### Molecular modelling

For the molecular modeling study, the fully hydrolyzed PVA fragment was constituted by $(PVA_{99})_{17}$. For the partially hydrolyzed one $(PVA_{87})_{14}$-$(PVAc)_3$, the sizes and repetitive units were chosen based on the proportion of and improvement of the F127 used $(PEO)_5$-$(PPO)_3$-$(PEO)_5$. The size of the chains was chosen to produce a lower computational cost of the equipment used. The complete fragment was used for optimization of the CA structure (Figure 2a). The optimized structures are shown in Figure 2b with the orientation of the PEO group (green), contrary to the PPO group (pink). The formation of the F127 micelle is highly dependent on the medium in which it is found, with separation between the nucleus and the corona evidenced. Albano *et al.*[40] have already reported, by dynamic modeling using water as a solvent, the formation of U-shaped lamellae, with the direction of the PEO tails facing the same direction. The same can be observed for those found in this work (Figure 2b), with the orientation of the PEO group (green) contrary to the PPO group (pink).

The different conformations of $PVA_{99}$ are presented in Figures 3a-3c. The structure in Figure 3b provided lower energy; therefore, taken at 0.00 kcal $mol^{-1}$, it features a polymeric chain with interacting hydroxyls and a very evident geometric tension. For the structure with $PVA_{99}$ hydroxyls and dispersed hydrogen bonds, a higher energy of 19.88 kcal $mol^{-1}$ is observed compared to Figure 3b.

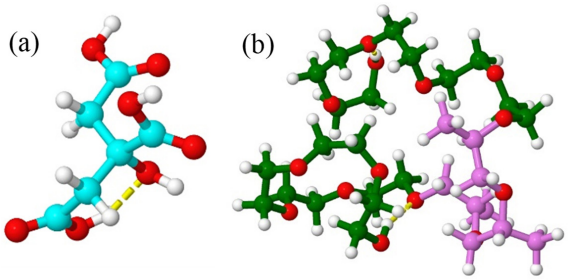


**Figure 2.** Structures optimized for (a) citric acid and (b) F127.

For Figure 3c, a linear structure can be observed for hydrogen interactions between the hydroxyl groups along the chain, still an energy of 14.07 kcal $mol^{-1}$ higher than Figure 3b. For $PVA_{87}$, the different orientations of the vinyl acetate (VAc) clusters and their location in the chain were evaluated. The different degrees of hydrolysis of PVA come from the hydrolysis (methanolysis) of PVAc, so it is impossible to define the locality in the chain of the VAc clusters correctly. In our work, the addition of VAc at the ends, center, and dispersed along the chain was evaluated, as shown in Figures 3d-3f.

A linear structure is formed for VAc grafted at the PVA chain's center (Figure 3d) and end (Figure 3e). In the case of the structure Figure 3d, hydrogen interactions are dispersed along the chain, making this structure possess an energy of 12.57 kcal $mol^{-1}$ more when compared to the structure Figure 3e, which presents the VAc at the end. Note the presence of hydrogen interactions along the entire chain, which makes the structure Figure 3e most stable, with lower energy and therefore, defined as energy 0.00 kcal $mol^{-1}$. The insertion of VAc dispersed along the PVA chain (Figure 3f) forms a structure with a slight twist, resulting from the repulsion between the carbonyl double bonds present in the structure, making its energy 31.08 kcal $mol^{-1}$ above the structure Figure 3e.

To observe the possible differences in the interactions between the polymer chains, an optimization was performed with two chains, designated as $2PVA_{87}$ and $2PVA_{99}$ (Figures 4a and 4b). For complexation, the inter-chain interaction is better tuned; thus, chains that maximize these interactions are favored. $2PVA_{99}$ (Figure 4b) provides a high interaction energy due to hydroxyls' inter-chain hydrogen interactions. On the other hand, $2PVA_{87}$ (Figure 4a) decreases these interactions due to the presence of acetal groups; this provides a lower interaction energy than $2PVA_{99}$. Furthermore, $2PVA_{99}$ (Figure 4b) has more intra and intermolecular hydrogen interactions with different orientations than $2PVA_{87}$ (Figure 4a). The presence of acetal groups decreases intra- and inter-chain bonds, providing greater mobility at the end to which they are attached and a slight twist at the opposite end. Hydrogen interactions

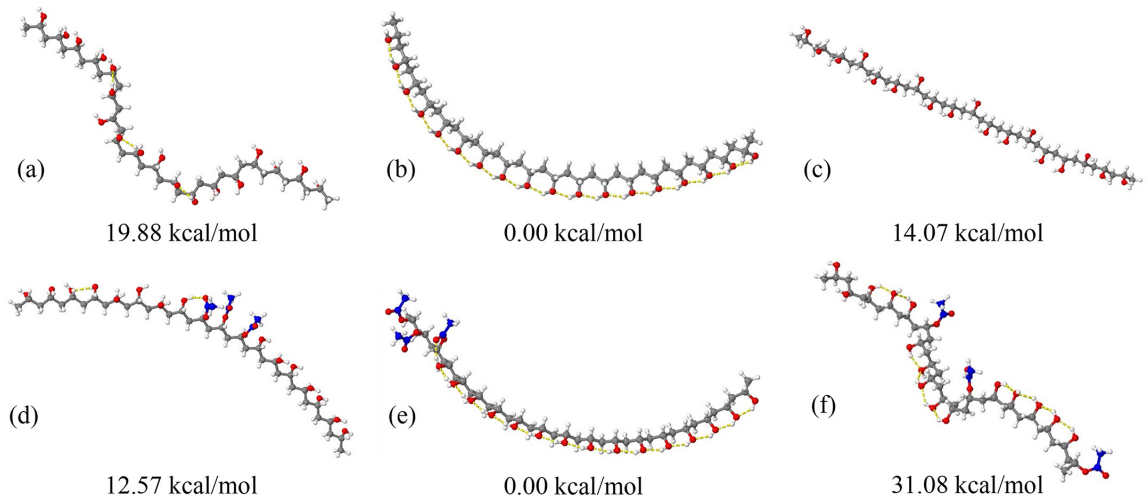


**Figure 3.** $PVA_{99}$-optimized structures in (a), (b), (c), and $PVA_{87}$-optimized structures with VAc (blue) fragments at (d) center, (e) end, and (f) scattered along the chain.

can provide different physicochemical characteristics to PVA, such as solubility and stability in water, viscosity, crystallinity, and melting temperature.[41] Also, the hydroxyl groups along the chain can incorporate other molecules by hydrogen bonding.[42]

The addition of the citric acid crosslinker between the polymer chains was also observed in Figures 4c and 4d. The PVA structures with the highest interaction energy with CA differ from those previously shown. Citric acid is a polycarboxylic acid with three carboxyl groups and can bind to the hydroxyl groups of PVA through inter and intramolecular interactions, forming crosslinking between the chains. Crosslinking reduces the available hydroxyl groups of PVA and, therefore, manages to decrease its hydrophilic nature.[18] For both DH and PVA, the formation of hydrogen interactions between the hydroxyl groups of the polymer and the acetal groups of the CA were observed. Another feature observed is the formation of multiple hydrogen bonds between CA and PVA in both degrees of hydrolysis. Numerous hydrogen bonds indicate more excellent molecular stability.[43] CA benefits from structural distortions to act as cavities and increase its interaction with the polymer. For $2PVA_{87}$/CA (Figure 4c), the CA settles between the polymeric chains, making them more

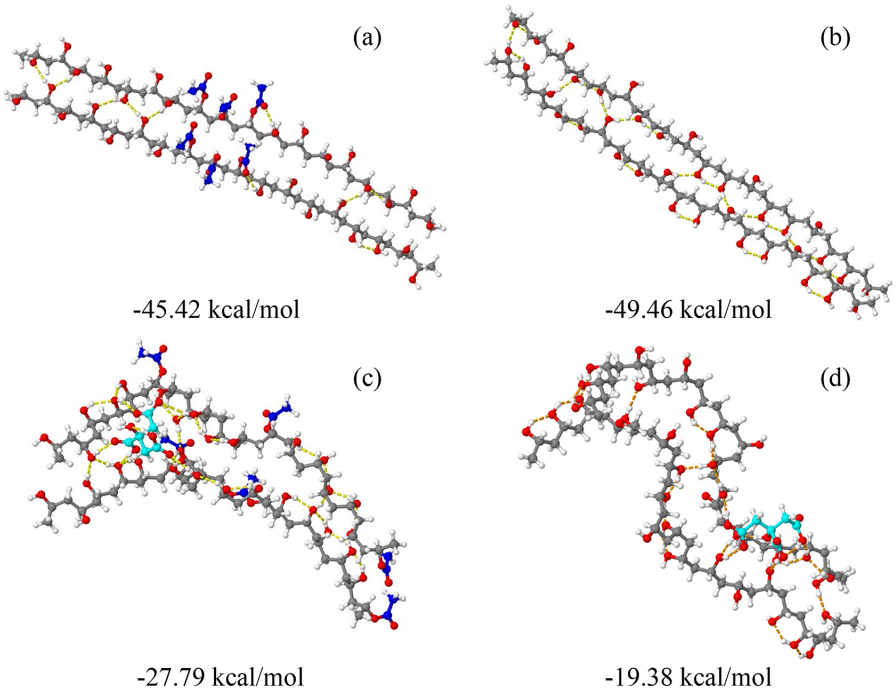


**Figure 4.** Optimized structure of (a) $2PVA_{87}$, (b) $2PVA_{99}$, (c) $2PVA_{87}$/CA and (d) $2PVA_{99}$/CA.

spaced. For $2PVA_{99}$/CA (Figure 4d), it is observed that the CA does not graft between the polymer chains. $PVA_{99}$'s stronger hydrogen interactions can explain this; therefore, its higher rigidity slightly distorts the structure to increase its interaction.

Adding F127 to structures already optimized with citric acid provides different results when comparing the other DH (Figure 5). For $2PVA_{87}$/CA/F127 (Figure 5a), contrary to expectations, F127 interacts more strongly with citric acid. Possibly, the acetal groups need to allow the effective approximation of the voluminous structure of the F127 with the polymeric structure. In this case, the interaction with the polar groups of the CA becomes more stabilizing. For $2PVA_{99}$/CA/F127 (Figure 5b), the F127 fragment is located opposite the CA and linked to the polymer by hydrogen bonds.

Table S1 (Supplementary Information (SI) section) shows the energy minima of the studied structures and fragments. To better understand better the interaction between the PVA chains and with the addition of CA and F127, it was used as a favorable parameter. The values of $2PVA_{87}$/CA and $2PVA_{99}$/CA in different DHs show that the interactions are suitable for the complexation of PVA with CA, explained by $\Delta E_{comp} < 0$. Compared to each other, the insertion of CA between the polymer chains is more favorable for $PVA_{99}$ ($\Delta E_{comp} = -60.25$ kcal mol$^{-1}$) once your energy is smaller than for $PVA_{87}$ ($\Delta E_{comp} = -39.05$ kcal mol$^{-1}$). The fragments interaction regards the mixing of the fragments electronic orbitals and the electrostatic interaction resulting from the charge polarization caused by the polar substituents, in this case, VAc and OH.[44] Because of the shape of the orbitals and the position of the substituents on the fragment frame, the electronic interaction becomes highly directional meaning that it strongly depends on the direction one fragment approaches the other. Larger negative values means that the electronic interaction is stronger, the geometry of the fragment is optimized and closer to the real one. This approach is used to describe a variety of chemical problems such as the interaction mode between catalyst and substrate,[45,46] amino acids interactions,[47,48] regioselectivity and reaction path elucidation.[49-52]

## Evaluation of interactions by NCI

For the conformation of $2PVA_{99}$/CA/F127 of lower energy, no evident interactions of F127 with PVA were observed; therefore, we sought to evaluate the types of interactions that occurred in this PVA/CA/F127 system in both DH. The method used was the Non-Covalent Interaction index (NCI), which uses electronic density and its derivatives to demonstrate attractive and repulsive interactions through isosurfaces with color scale.[53] RGB (red-green-blue) is used for the NCI to elucidate the dispersive interactions of small molecules and complexes.[54] This approach describes those regions in red that present repulsive/destabilizing interactions, while in green, a low number of electrons and weak delocalized interactions, and finally, in blue, the attractive/stabilizing interactions.[53,54] For $2PVA_{87}$/CA/F127 and $2PVA_{99}$/CA/F127, both weak interactions and strong stabilizing interactions were verified in the presence of F127 and CA in both DH. Their isosurfaces are shown in Figure 6.

The NCI analyses (Figure 6) or DH demonstrate a similar pattern of interactions with the presence of regions located in dark blue between oxygens of the acidic hydrogens of CA and PVA and a large area in green for the exchange of F127 with PVA. F127, on the other hand, does not present hydrogen interactions as intense as CA. However, it is possible to observe light blue regions between the oxygens of F127 and the acidic hydrogens of PVA and/or CA, indicating weaker hydrogen interactions. The large green area between F127 and the other structures demonstrates that dispersive interactions play a significant role in stabilizing this complex; the fact that this area is more prominent for $PVA_{99}$ is consistent with the higher interaction energy shown. In this way, with this computational tool, the explanations regarding the properties of the solution become more coherent.

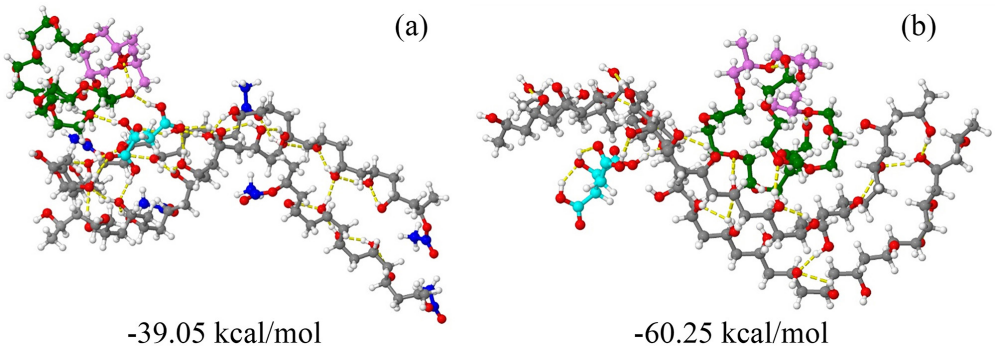


**Figure 5.** Structures optimized for (a) $2PVA_{87}$ and (b) $2PVA_{99}$, both with CA (cyan) and F127 (green and pink).

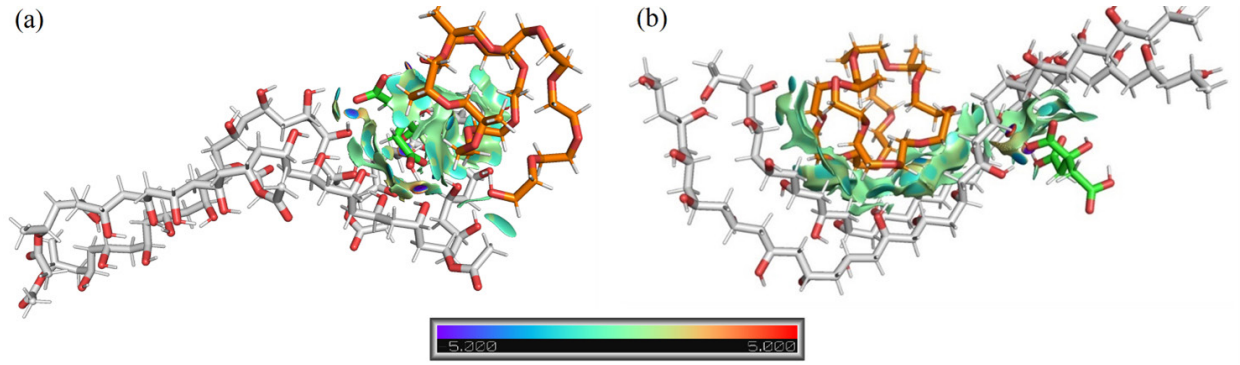


**Figure 6.** NCI isosurface for the (a) $PVA_{99}$/F127/CA and (b) $PVA_{87}$/F127/CA, where the color of the PVA chain is gray, the CA structure is green and the entire F127 is orange.

## Solution properties

The electrical conductivity of an electrospinning solution plays a significant role in the average fiber diameter. Initially, it can be observed in Table S2 (SI section) that the DH provides different conductivities. For $PVA_{99}$, the conductivity is 1203.09 ± 6.65 μS $cm^{-1}$, while for $PVA_{87}$, 950.33 ± 4.56 μS $cm^{-1}$. These data were also reported by Zhang *et al.*[55] which indicate that the increase in DH at the same polymer concentration leads to an increase in the conductivity of the solution due to aggregation and crystallization occurring at the air/solution interface. The addition of CA to $PVA_{87}$ and $PVA_{99}$ solutions in all evaluated conditions leads to an increase in conductivity, explained by the ionizable nature of the acid. CA is a weak electrolyte, with fractions of positively and negatively charged ions in solution. Similar data were found by Shi and Yang.[56]

In addition to electrical conductivity, rheology has been used to predict electrospinning solution properties by providing morphological correlation and spinning ability. Analyzing the flow behavior (Figure 7a) for $PVA_{87}$ and $PVA_{99}$ solutions makes it possible to verify a representation of a non-Newtonian fluid. A non-Newtonian fluid is characterized by a fluid behavior independent of when the shear stress is applied.[57] Another feature that can be observed is pseudoplastic behavior. Pseudoplastic fluids have a convex curvature about the shear gradient axis starting from zero, yet they are solutions that have chains in an entangled state and, under shear stress, tend to orient themselves in the direction of the applied force, decreasing their apparent viscosity.[57,58] When comparing the polymers in different degrees of hydrolysis, it is possible to denote that the $PVA_{99}$ Figure 7b tends to undergo more significant changes in viscosity as the force is applied.

Still, in Figure 7b, it is also possible to observe that $PVA_{99}$ has an initial viscosity 40% higher than that of $PVA_{87}$. The viscosity of PVA is closely related to the intra and inter-molecular hydrogen bonds of the chains. For $PVA_{99}$, interactions and chain entanglement are more pronounced when compared to $PVA_{87}$, which has acetate groups that manage to interrupt inter- and intra-chain hydrogen bonds, corroborating the results found in Figure 4b, thus having a lower apparent viscosity.[59] For $PVA_{87}$, a small hysteresis area is observed in the return curve, indicating that the solution is still fluid even after receiving a strain rate.

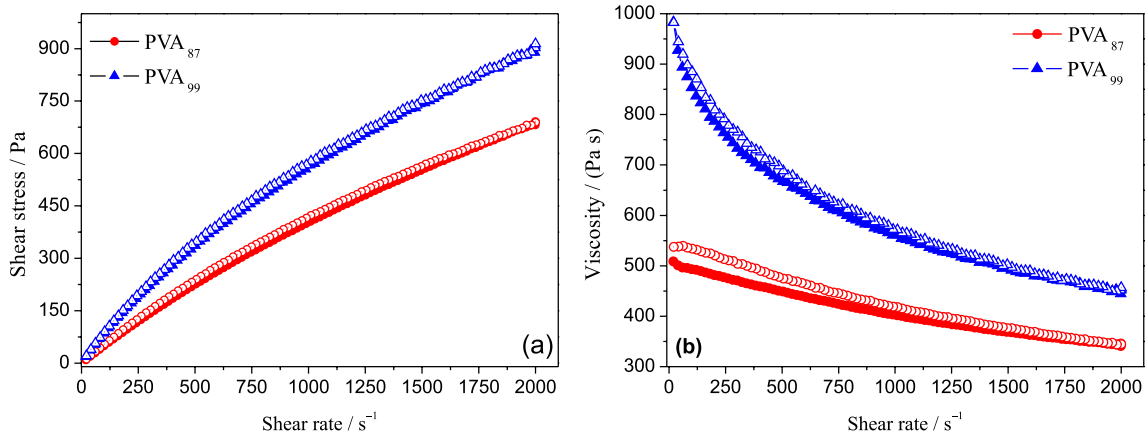


**Figure 7.** Rheogram of (a) flow and (b) viscosity for $PVA_{87}$ and $PVA_{99}$ solutions in aqueous medium. The closed symbol represents the one-way curve, and the open symbol represents the turn.

For the $PVA_{87}$ solutions in the flow rheogram of Figure 8a, adding F127 and different percentages of CA still give predominantly non-Newtonian fluid characteristics, behaving like pseudoplastic. The addition of CA alters the structural configuration of the solution, bringing it to a similar behavior to the pure $PVA_{87}$ solution; this behavior is in accordance with the analysis carried out in Figure 5a, in which, contrary to what was imagined, F127 interacts more strongly with citric acid. For the $PVA_{99}$ solution in the flow rheogram (Figure 8b), the addition of F127 and different percentages of CA also maintains the non-Newtonian fluid characteristics of PVA, and these solutions behave like pseudoplastics. Contrary to the data found for PVA87, the addition of F127 decreases the dependence of the $PVA_{99}$ solution on the shear rate, indicating that the viscosity of the solution does not change significantly when a force is applied. The addition of CA alters the structural configuration of the solution, as reported in the analysis of $PVA_{99}$/CA/F127 (Figure 5b). The fragment of F127 is located in the opposite position to the CA and connected to the polymer by hydrogen bonds, promoting this conformational modification.

When analyzing the apparent viscosity of the solutions shown in Figure 8c, it is possible to notice that the $PVA_{87}$/F127 solution is shear-dependent since its viscosity decreases with the increase of the gradient. For the $PVA_{87}$/F127 solutions with the addition of CA, there is a decrease in the apparent viscosity with the increase in the shear gradient, reaching a viscosity close to that of the pure $PVA_{87}$ solution. The interactions of PVA with CA occur through the hydroxyl and carboxylic groups present in the acid. The three carboxylic groups present in CA increase the formation of hydrogen bonds through esterification with the hydroxyl groups of PVA.[60] $PVA_{99}$ solutions, as shown in Figure 8d, exhibit different apparent viscosity behavior than $PVA_{87}$ when F127 and different mass percentages of CA in the solution are inserted. As we saw in Figure 4b, $PVA_{99}$ has many inter- and intrachain interactions, and the insertion of CA can cause a break in the sequence of these interactions and hydrogen bonds, according to Figure 5b.

Table S3 (SI section) presents the rheological data for the different formulations of solutions for electrospinning, such as consistency index (k), flow behavior index (n), yield value ($\tau_0$), and thixotropy area ($A_t$) calculated using

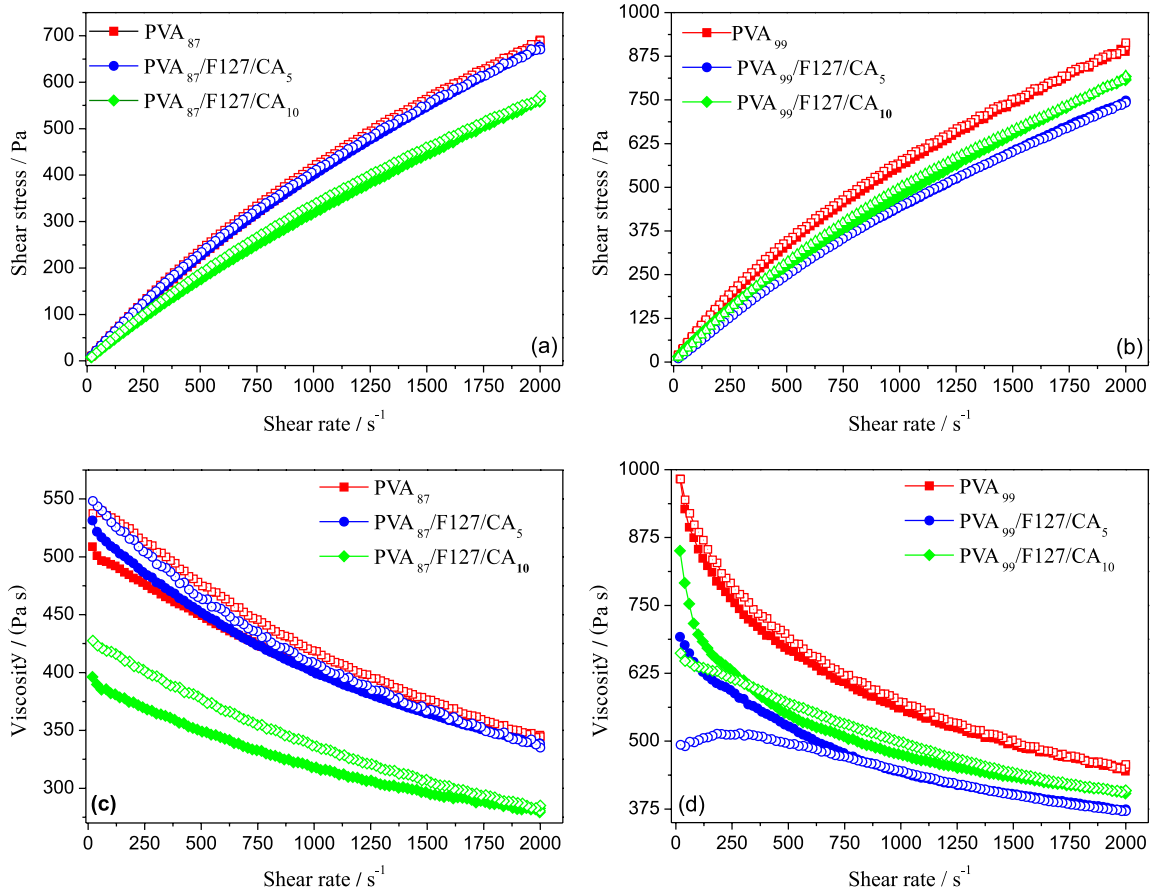


**Figure 8.** Rheogram of flow for (a) $PVA_{87}$ with the insertion of F127 /CA and (c) $PVA_{99}$ with the insertion of F127 /CA. Rheogram of viscosity for (c) $PVA_{87}$ with the insertion of F127 /CA and (d) $PVA_{99}$ with the insertion of F127 /CA. The closed symbol represents the one-way curve, and the open symbol represents the turn.

equations 4, 5, and 6. k represents the average viscosity of all points obtained by a flow curve. The highest value of $PVA_{87}$ solutions was obtained with the insertion of F127, which is related to the increased viscosity discussed above. For $PVA_{99}$, the lowest value was also obtained by inserting F127. The data then agrees with the rheograms in Figures 7a and 8d. The flow behavior index (n) represents the shear dilution behavior, where n = 1, we have a Newtonian fluid, n < 1 pseudoplastics, and n > 1 dilatants.[61] All solutions obtained values of n smaller than 1, able to be classified as pseudoplastic, and tend to have their viscosity reduced with the increase of the shear stress. These results are in accordance with the rheograms shown in Figures 7a and 8a-8b. The thixotropy area is calculated using the hysteresis area, evaluating the structural organization before and after shear conditions.[62] All solutions studied showed rheological behavior of rheopexy (negative $A_t$), indicating a slower system reorganization after suffering a high shear rate deformation.[63] The data in align with those already reported in the viscosity rheograms (Figures 7b, 8c and 8d).

### Properties of the electrospun matrix

The structural and morphological effects caused by the electrospun matrices of $PVA_{87-99}$/F127 with the addition of different percentages of CA mass after heat treatment were evaluated by SEM. PVA/F127 concentrations were maintained at 9% by mass, with a ratio of 8:1. The electrospun matrix morphology of $PVA_{87}$ is shown in Figure 9a with average size fibers of 300 ± 58 nm of random distribution and flattened structure. The flattened morphology of PVA fibers has also been reported by Koski *et al.*[64] The authors attest that high humidity and impact form this structure when reaching the collector. For the $PVA_{99}$ solution, forming a film on the target collector was impossible. Koski *et al.*[64] elucidated the relationship between the molecular weight of $PVA_{99}$ and the concentration of the solution for the formation of homogeneous fibers. Using the Mark-Houwink relationship and relating the intrinsic viscosity to the concentration, the authors demonstrated that a solution with a mass proportion of 6% $PVA_{99}$ can form fibers. Yao *et al.*[65] indicate that the surface tension of the PVA solution is related to the degree of hydrolysis. For $PVA_{99}$, the high surface tension needs critical electric fields well above 30 kV to form a stable Taylor cone. The authors indicate using non-ionic surfactants to decrease the surface tension of aqueous $PVA_{99}$ solutions.

Initially, when analyzing the images of $PVA_{87}$/F127 nanofibers (Figure 9b), it can be seen that they have a uniform morphology and a crimped characteristic. El-Aassar *et al.*[24] report that the concentration of F127 plays an essential role in the formation of $PVA_{87}$ fibers, which cannot exceed 1% by mass and, when compared to pure PVA fibers, tend to favor the formation of friezes. The fibers tend to merge with the addition of CA (Figures 9c and 9d). Coalescence can occur when there is close contact between the threads or when they cross, producing a joint geometry.[66] Wang and Hsieh[67] observed that the addition of a cross-linker to PVA/polyethylene

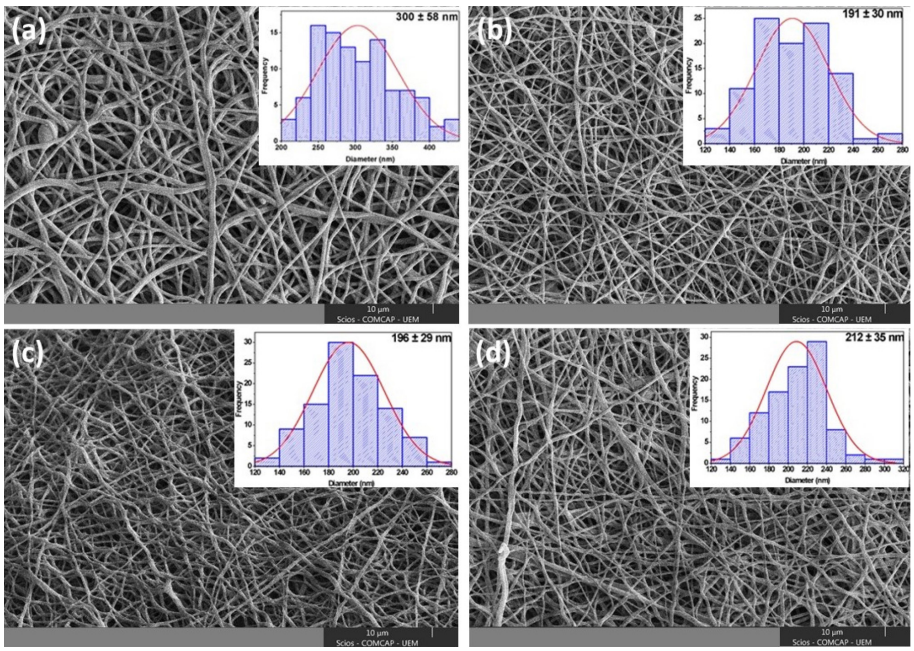


**Figure 9.** Morphology of electrospun matrices and fiber diameters after heat treatment of (a) $PVA_{87}$, (b) $PVA_{87}$/F127, (b) $PVA_{87}$/F127/$CA_5$, and (c) $PVA_{87}$/F127/$CA_{10}$.

glycol (PGE) fibers, with a molar mass similar to that of this work, led to the formation of coalescing fibers with reduced porosity when compared to PVA/poly(ethylene glycol)(PEG), explained by the compaction of the fiber structure. When comparing the average histogram fiber diameters for each composition, it is observed that $PVA_{87}$/F127 (Figure 9b) has a diameter distribution of 191 ± 30 nm. When comparing the diameter with pure PVA (Figure 9a), there is a reduction of 51.33% in the diameter with the insertion of F127 in the polymeric solution, and the decrease in viscosity can explain these data. Zadeh *et al*.[68] point out that solvent evaporation is reduced with increasing viscosity, forming fibers with a larger diameter. With the addition of CA (Figures 9c and 9d), there was a slight increase in the average diameter of the fibers; however, when considering the standard deviation, it is impossible to denote significant differences. Nataraj *et al*.[20] also observed a 10-150 nm change in the diameter of low molar weight PVA fibers (44.05 g $mol^{-1}$) when crosslinked with 5% CA. The conductivity provided by the CA was essential for forming fibers with a circular cross-section since the viscosity of the PVA/F127/CA solutions is very close to that of pure PVA. The data obtained from average diameters align with the rheology and conductivity data of the solution.

Microscopies for the $PVA_{99}$ solutions (Figure 10Aa) demonstrate that solvent evaporation is incomplete. For the dissolution of PVA with a high degree of hydrolysis, temperatures above 110 °C should be used to break the inter- and intra-chain bonds in more significant numbers, as seen in Figure 4b. These bonds can be redone with the cooling of the solution or during the path to the target collector, causing the evaporation rate of the solvent from the formed gel structure to be drastically reduced.[64] As previously reported, the viscosity of the solution is also closely linked with the evaporation of the solvent along the path to the target collector. When comparing the additions of CA, the one with 5% provided a better chance of fiber formation due to lower viscosity. This data agrees with those of rheology previously presented in Figure 8d. The high viscosity of the solutions for adding 10% CA and a slow solvent evaporation rate meant that the material still arrived highly wet at the target collector, ultimately losing its fiber characteristic.

To circumvent the limitation of $PVA_{99}$, binary solvents for electrospinning have already been studied. Mahmud *et al*.[69] evaluated the effect caused by the electrospinning of PVA (115 KDa, DH 98.99%) with ethanol-water mixtures (20 and 50%) and acetic acid-water (20 and 50%). The authors verified the formation of circular fibers with 7% PVA and the acetic acid-water mixture and flat fibers for the same concentration using ethanol-water. Furthermore, larger diameters were observed for solutions using ethanol-water (500-1000 nm) as a solvent than acetic acid-water (70-300 nm). For PVA (125 KDa and DH 86-89%), it has been reported that adding up to 40% dimethyl sulfoxide (DMSO) can provide uniform formation and fibers; however, the high-water content in the solution must be maintained for optimum spinning ability.[70] The addition of 20 and 30%

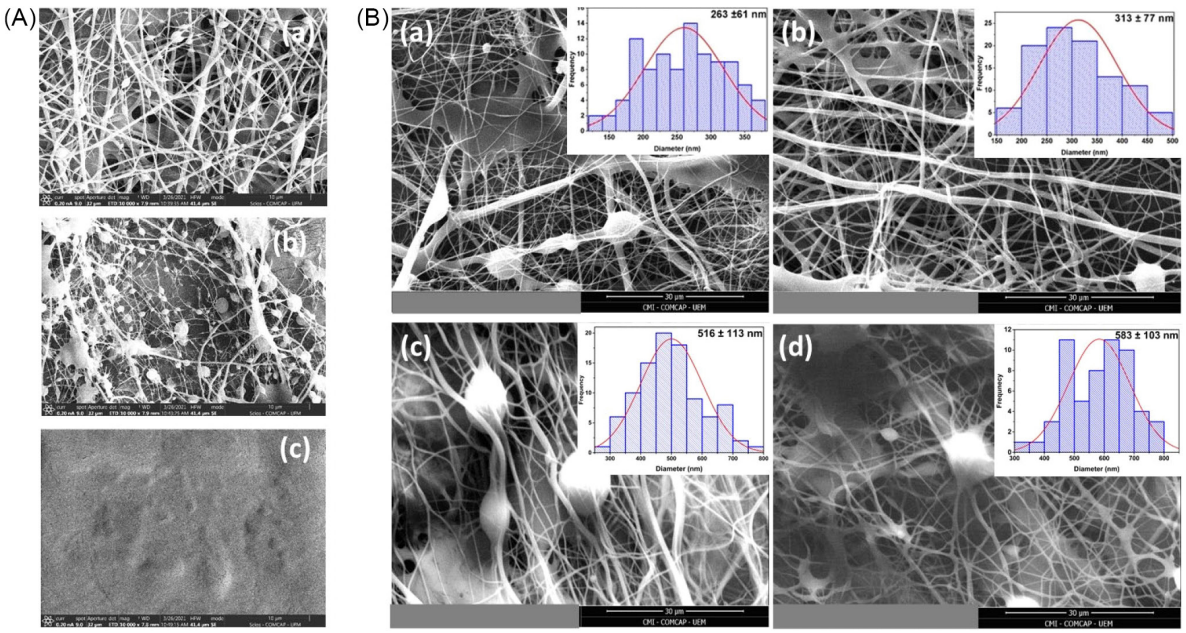


**Figure 10.** Morphology of electrospun matrices of (A) (a) $PVA_{99}$/F127 (b) $PVA_{99}$/F127/$CA_5$ and (c) $PVA_{99}$/F127/$CA_{10}$. (B) (a) $PVA_{99}$-20%Aace, (b) $PVA_{99}$-30%AAce (c) $PVA_{99}$/F127/$CA_5$/30%AAce and (d) $PVA_{99}$/F127/CA10/30%AAce.

acetic acid (AAce) to the $PVA_{99}$ solution was evaluated; the microscopies are shown in Figure 10B. Adding 20% of AAce (Figure 10Ba) favors the formation of fibers with average diameters of 263 ± 61 nm, with the predominance of beads and polymer agglomerate coming from a slow evaporation rate. For the addition of 30% AAce in Figure 10Bb, more homogeneous fibers were observed, with an average diameter of 313 ± 77 nm, but still with the presence of polymer agglomerate in a smaller amount. Starting from the addition of 30% AAce to the solution, with the production of better fibers for $PVA_{99}$, electrospinning was performed with solutions containing F127 and CA in the same proportions already reported.

Microscopies for adding F127 and CA (Figures 10Bc and Bd) show that it does not promote the formation of homogeneous and regular fibers, even with the binary mixture of solvents. For this solution configuration (PVA/F127/CA) and PVA (Mw 146.000-186.000, +99% hydrolyzed), no studies were reported in the literature, this being the first to address this system. We believe that, as shown in Figure 5b (system only in water), the hydrogen interactions are still strong for $PVA_{99}$ in binary solution, making the surface tension and tendency to undergo gelation higher, as reported by Park *et al.*[71] In a systematic review, Matabola *et al.*[72] indicate that adding surfactants and co-solvents can help electrospinning PVA in high DH; however, no success reports were found. Other observations are the high standard deviation between measurements, confirming Taylor Cone's instability and fibers of different diameters.

Our findings indicate that the addition of acetic acid to the PVA electrospinning solution improves the formation of nanofibers by reducing the surface tension and viscosity of the solution, which facilitates the electrospinning process. Specifically, the use of 30% acetic acid resulted in more homogeneous fibers with fewer defects compared to using water alone. This is consistent with the findings reported by Mahmud *et al.*,[69] who demonstrated that acetic acid enhances the electrospinning performance and morphological characteristics of PVA nanofibers. In our experiments, we observed that the $PVA_{87}$/F127/CA system produced fibers with a uniform morphology and a crimped characteristic when acetic acid was used as a solvent. The average fiber diameter was significantly reduced, which can be attributed to the decreased viscosity and improved electrospinning conditions. These results align with the study by Vu *et al.*,[73] which reported that acetic acid does not affect the chemical properties of PVA nanofibers but changes their lattice structure and reduces crystallinity.

The chemical and structural characterization of the $PVA_{87}$ and $PVA_{99}$ membranes after heat treatment (HT) were performed by Raman spectroscopy and is shown in Figure 11. Behavioral differences were observed in the assigned bands. For the band corresponding to O–H stretching, a significant reduction is marked with the addition of CA+ HT to $PVA_{87}$ (Figure 11a), indicating a decrease in hydrogen bonds and crosslinking. An increase in CA concentration is observed for the band attributed to aliphatic C–$H_2$ stretching and $PVA_{87}$. Kim *et al.*[74] also observed this effect and attributed it to higher PVA crosslinking. For $PVA_{99}$ (Figure 11b), the observed effect was contrary to what was imagined, with increased OH and $CH_2$ stretching bands. As we saw in the molecular modeling study (Figure 5), for CA, there are still O–H groups that do not react with PVA and F127, causing an increase in intensity. Thus, this characterization makes it impossible to attest to the $PVA_{99}$ crosslinking for the studied system.

Thermogravimetric analysis (TGA) was used to evaluate the thermal decomposition of PVA/F127/CA fibers for both DH. Pure PVA membranes (Figures 12a and 12d) show three well-defined stages of decomposition. The first stage at 150 °C corresponds to the elimination of water chains.

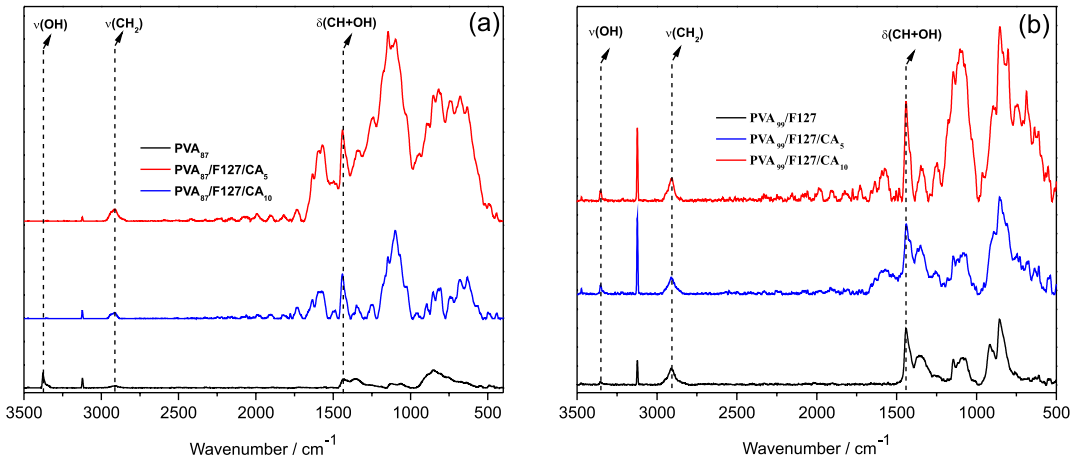


**Figure 11.** Raman spectroscopy for (a) $PVA_{87}$ and (b) $PVA_{99}$ membranes at different CA percentages.

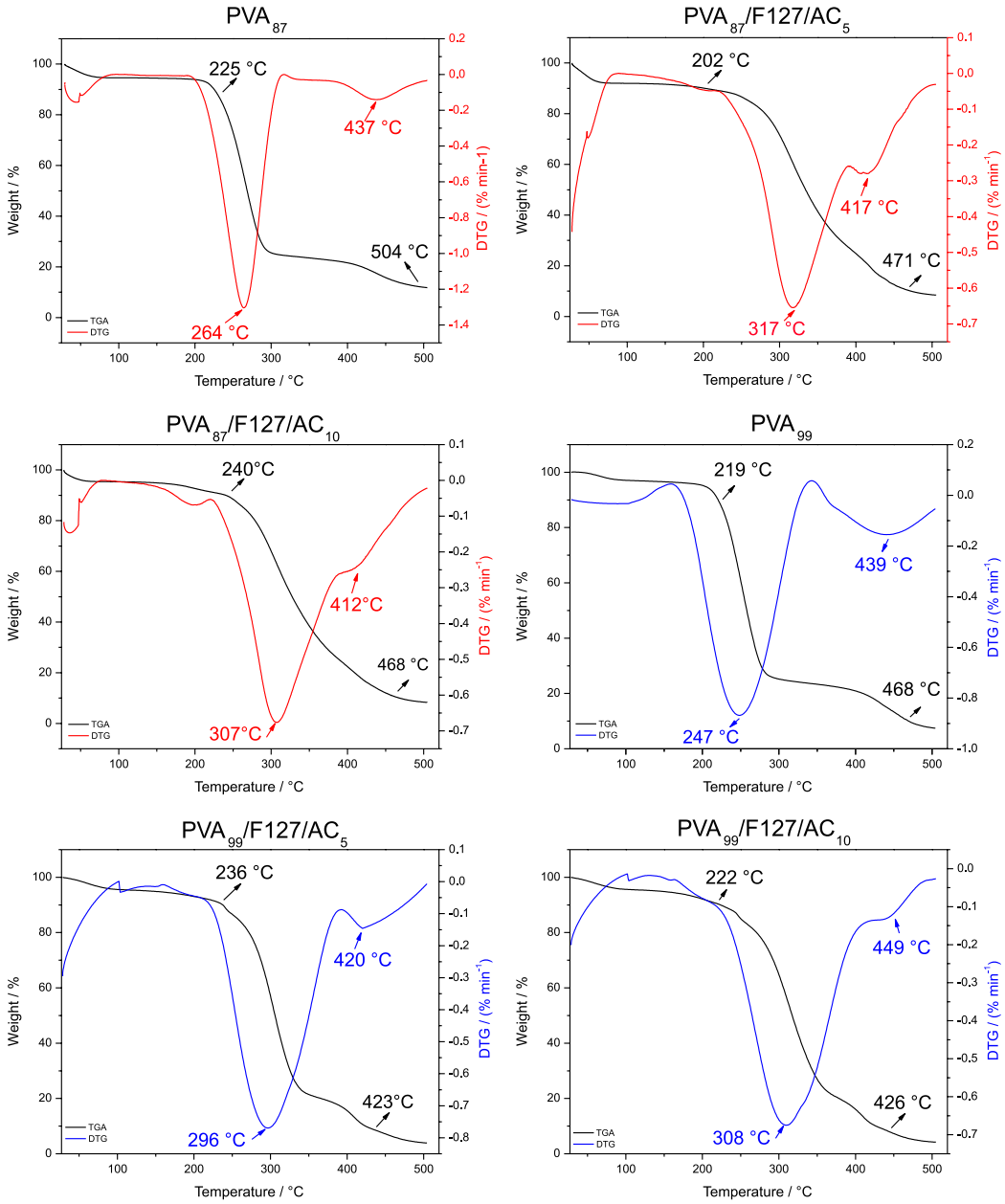


**Figure 12.** Thermogravimetric curves (TGA) and derivative of degradation curves (DTG) for (a) $PVA_{87}$, (b) $PVA_{87}$/F127/$CA_5$, (c) $PVA_{87}$/F127/$CA_{10}$, (d) $PVA_{99}$, (e) $PVA_{99}$/F127/$CA_5$ and (f) PVA99/F127/$CA_{10}$.

The second step near 250 °C involves eliminating hydroxyl side groups and forming small polyene fragments. The third stage, from 300 °C, corresponds to the decomposition of the PVA main chain.[75] The derivative thermogravimetry (DTG) curves (Figures 12a and 12d) demonstrate that the maximum decomposition of PVA in the second stage, for $PVA_{87}$, occurs at 264 °C and $PVA_{99}$ at 247 °C. The more excellent thermal stability of $PVA_{87}$ is related to the acetal groups present in the chains and the reduction of hydroxyl groups to undergo decomposition.[76] Inserting F127/CA increases the decomposition temperature for both PVAs, indicating crosslinking. This temperature corresponds to the three-dimensional network between PVA and CA, as shown in Figures 5a and 5b. When comparing the percentages of CA to the system, for $PVA_{87}$, the addition of 5% was more favorable, and for $PVA_{99}$, the addition of 10%. For $PVA_{99}$, as shown in Figure 5b, here are more points for three-dimensional network formation because CA accommodation is opposite to F127, and there is no presence of acetal groups. Also, the NCI isosurface (Figure 6b) demonstrates that the interaction of $PVA_{99}$ with F127 occurs along the entire chain; thus, a higher concentration of CA is expected to form a more stable three-dimensional network. For $PVA_{87}$, we believe the

acetal groups along the chain, as shown in Figure 5a, do not favor the entry of more CA into the structure and the formation of more crosslinking points; thus, excess CA causes the most pronounced degradation at 10 than 5%.

Stability in aqueous media was carried out for PVA/F127/CA10 in the two DHs studied, and the microscopies are presented in Figure 13. For $PVA_{87}$/F127/$CA_{10}$ (Figure 13a), the maintenance of the fibrous characteristic can be observed even after prolonged immersion in water, demonstrating crosslinking by CA. This fact corroborates the molecular modeling data (Figure 5a) and Raman spectroscopy (Figure 11a). Crosslinking with CA decreased water sorption by the fibers. For $PVA_{99}$/F127/$CA_{10}$ (Figure 13b), the fibrous characteristic of the material is almost completely lost, demonstrating the non-crosslinking of the material. Cross-linking of the material occurs when the OH groups of the CA provide inter and intramolecular interactions. From Figure 5a, it is observed that the addition of F127 decreases the effective bonds of CA with the polymer chains, which makes the crosslinking less effective. Furthermore, the increases in the signal of the OH groups in the Raman spectroscope Figure 12b also corroborate this observation.

Fraga *et al*.[21] verified the stability of smaller Mw $PVA_{99}$ membranes cross-linked with $CA_{10}$ after immersion in an aqueous medium for 24 h. do Nascimento *et al*.[77] also confirmed the stability of $PVA_{99}$ membranes with Mw equal to that used by us and crosslinked with CA. Therefore, the addition of F127 to the system can cause competition with CA for the active sites of the polymer, decrease the crosslinking efficiency, and increase water sorption.

## Conclusions

The study demonstrated that PVA with 99% degree of hydrolysis (DH) and high molar mass is unsuitable for electrospinning due to high viscosity and poor fiber formation. In contrast, PVA with 87% DH showed better results when crosslinked with citric acid (CA) and combined with Pluronic® F127 (F127). The molecular modeling confirmed that CA effectively crosslinks PVA, enhancing stability. Rheological data indicated non-Newtonian fluid behavior, with $PVA_{99}$ showing higher viscosity than $PVA_{87}$. SEM analysis revealed uniform fiber morphology for $PVA_{87}$/F127/CA, while $PVA_{99}$ solutions failed to form homogeneous fibers. TGA confirmed the crosslinking of $PVA_{87}$, but not $PVA_{99}$, as evidenced by thermal stability and residue analysis. Stability tests in aqueous media further validated the effective crosslinking of $PVA_{87}$/CA/F127. Thus, $PVA_{87}$/CA/F127 is a promising system for electrospun nanofibers, particularly for drug delivery applications.

## Supplementary Information

Supplementary data are available free of charge at http://jbcs.sbq.org.br as PDF file.

## Acknowledgments

The authors would like to thank the Nucleus for Research in Photodynamic Systems (NUPESP–UEM), the Interdisciplinary Group for Photochemical and Electrochemical Environmental Research (GIP&FEA-Unioeste) and Complexo de Centrais de Apoio à Pesquisa (COMCAP-UEM) for allowing the use of necessary equipment. ARSR acknowledges Coordenação de Aperfeiçoamento de Pessoal de Nível Superior (CAPES-Brazil) for her PhD fellowship.

### Author Contributions

Ariane Regina S. Rossin was responsible for formal analysis, investigation, writing original draft; Vinicius Martinelli for methodology, formal analysis, visualization; Ernani A. Basso for

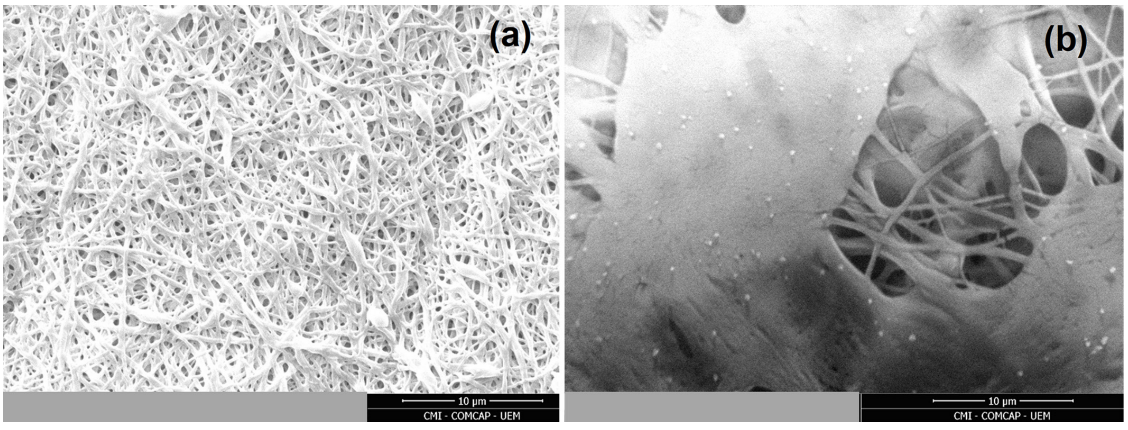


**Figure 13.** SEM images of (a) $PVA_{87}$/F127/$CA_{10}$ and (b) $PVA_{99}$/F127/$CA_{10}$ after immersion in water.

formal analysis, visualization; Mariana S. Gibin for methodology, formal analysis, visualization; Vitor S. Zanuto for methodology, formal analysis, visualization; Bruno Henrique Vilsinski for formal analysis, visualization; Eduardo Radovanovic for formal analysis, visualization; Wilker Caetano for formal analysis, visualization; Douglas C. Dragunski for conceptualization, investigation, supervision.

## References


1. Xue, J.; Wu, T.; Dai, Y.; Xia, Y.; *Chem. Rev.* **2019**, *119*, 5298. [Crossref]
2. Stace, E. T.; Mouthuy, P. A.; Carr, A. J.; Ye, H. C. In *Comprehensive Biotechnology*, vol. 5, 3rd ed.; Moo-Young, M., ed.; Pergamon: Amsterdam, 2019, p. 424. [Crossref]
3. Foong, C. Y.; Wirzal, M. D. H.; Bustam, M. A.; *J. Mol. Liq.* **2020**, *297*, 111793. [Crossref]
4. Augustine, R.; Rehman, S. R. U.; Ahmed, R.; Zahid, A. A.; Sharifi, M.; Falahati, M.; Hasan, A.; *Int. J. Biol. Macromol.* **2020**, *156*, 153. [Crossref]
5. Ramakrishna, S.; Fujihara, K.; Teo, W.-E.; Lim, T.-C.; Ma, Z.; *An Introduction to Electrospinning and Nanofibers*; World Scientific Publishing Co. Pte. Ltd: New Jersey, London, Singapore, Beijing, Shanghai, Hong Kong, Taipei, Chennai, 2005.
6. Nasouri, K.; *Polym. Test.* **2018**, *69*, 499. [Crossref]
7. Nezbeda, I.; Jirsák, J.; Moučka, F. In *Electrospun Nanofibers*; Afshari, M., ed.; Elsevier, 2017, ch.11. [Crossref]
8. Yousefzadeh, M. In *Electrospun Nanofibers*; Afshari, M., ed.; Elsevier, 2017, ch.12. [Crossref]
9. Lu, C.; Chen, P.; Li, J.; Zhang, Y.; *Polymer* **2006**, *47*, 915. [Crossref]
10. Vao-soongnern, V.; *J. Polym. Res.* **2019**, *26*, 147. [Crossref]
11. Aslam, M.; Kalyar, M. A.; Raza, Z. A.; *Polym. Eng. Sci.* **2018**, *58*, 2119. [Crossref]
12. Baker, M. I.; Walsh, S. P.; Schwartz, Z.; Boyan, B. D.; *J. Biomed. Mater. Res., Part B* **2012**, *100B*, 1451. [Crossref]
13. Gaaz, T. S.; Sulong, A. B.; Akhtar, M. N.; Kadhum, A. A. H.; Mohamad, A. B.; Al-Amiery, A. A.; McPhee, D. J.; *Molecules* **2015**, *20*, 22833. [Crossref]
14. Filova, B.; Musilova, L.; Mracek, A.; Ramos, M. L.; Veríssimo, L. M. P.; Valente, A. J. M.; Ribeiro, A. C. F.; *J. Mol. Liq.* **2020**, *304*, 112728. [Crossref]
15. Yang, E.; Qin, X.; Wang, S.; *Mater. Lett.* **2008**, *62*, 3555. [Crossref]
16. Liao, H.; Liu, Y.; Wang, Q.; Duan, W.; *J. Appl. Polym. Sci.* **2018**, *135*, 46402. [Crossref]
17. Salihu, R.; Abd Razak, S. I.; Ahmad Zawawi, N.; Rafiq Abdul Kadir, M.; Izzah Ismail, N.; Jusoh, N.; Riduan Mohamad, M.; Hasraf Mat Nayan, N.; *Eur. Polym. J.* **2021**, *146*, 110271. [Crossref]
18. Gautam, L.; Warkar, S. G.; Ahmad, S. I.; Kant, R.; Jain, M.; *Polym. Eng. Sci.* **2022**, *62*, 225. [Crossref]
19. Birck, C.; Degoutin, S.; Tabary, N.; Miri, V.; Bacquet, M.; *eXPRESS Polym. Lett.* **2014**, *8*, 941. [Crossref]
20. Nataraj, D.; Reddy, R.; Reddy, N.; *Eur. Polym. J.* **2020**, *124*, 109484. [Crossref]
21. Fraga, G. N.; Dragunski, D. C.; Vilsinski, B. H.; Azevedo, C. K. S.; Wiggers, H. J.; Faria, M. G. I.; Caetano, J.; da Costa, M. R.; Zanuto, V. S.; Rossin, A. R. S.; Gibin, M. S.; *Colloids Surf., A* **2023**, *674*, 131760. [Crossref]
22. Pelegrino, M. T.; de Araújo, D. R.; Seabra, A. B.; *J. Drug. Delivery Sci. Technol.* **2018**, *43*, 211. [Crossref]
23. Nascimento, M. H. M.; Franco, M. K. K. D.; Yokaichyia, F.; de Paula, E.; Lombello, C. B.; de Araujo, D. R.; *Int. J. Biol. Macromol.* **2018**, *111*, 1245. [Crossref]
24. El-Aassar, M. R.; El fawal, G. F.; El-Deeb, N. M.; Hassan, H. S.; Mo, X.; *Appl. Biochem. Biotechnol.* **2016**, *178*, 1488. [Crossref] [PubMed]
25. da Silva Jr., R. C.; Campanholi, K. S. S.; de Morais, F. A. P.; Pozza, M. S. S.; dos Santos, G. T.; Hioka, N.; Caetano, W.; *Dyes Pigm.* **2019**, *167*, 204. [Crossref]
26. Rwei, S. P.; Huang, C. C.; *Fibers Polym.* **2012**, *13*, 44. [Crossref]
27. Libel, G. P.; Facchi, S. P.; de Almeida, D. A.; Madruga, L. C.; Kipper, M. J.; Schrekker, H. S.; Martins, A. F.; Radovanovic, E.; *Mater. Chem. Phys.* **2024**, *316*, 129087. [Crossref]
28. Cornell, T.; Hutchison, G.; *Avogadro*, version 1.2.0; University of Pittsburgh, USA, 2017; Hanwell, M. D.; Curtis, D. E.; Lonie, D. C.; Vandermeersch, T.; Zurek, E.; Hutchison, G. R.; *J. Cheminf.* **2012**, *4*, 17. [Link] accessed in November 2024
29. Neese, F.; *ORCA*, v.5.0.; Germany, 2022; Neese, F.; Wiley, J.; *Wiley Interdiscip. Rev.: Comput. Mol. Sci.* **2012**, *2*, 73. [Crossref]
30. Grimme, S.; Bannwarth, C.; Shushkov, P.; *J. Chem. Theory. Comput.* **2017**, *13*, 1989. [Crossref] [PubMed]
31. Weigend, F.; Furche, F.; Ahlrichs, R.; *J. Chem. Phys.* **2003**, *119*, 12753. [Crossref]
32. Ernzerhof, M.; Scuseria, G. E.; *J. Chem. Phys.* **1999**, *110*, 5029. [Crossref]
33. Grimme, S.; Antony, J.; Ehrlich, S.; Krieg, H.; *J. Chem. Phys.* **2010**, *132*, 154104. [Crossref]
34. Marenich, A. V.; Cramer, C. J.; Truhlar, D. G.; *J. Phys. Chem. B* **2009**, *113*, 6378. [Crossref]
35. Zhang, J.; Dolg, M.; *Phys. Chem. Chem. Phys.* **2015**, *17*, 24173. [Crossref]
36. Zhang, J.; *ABCluster*, v.2.0; Republic of China, 2015.
37. Contreras-García, J.; Johnson, E. R.; Keinan, S.; Chaudret, R.; Piquemal, J. P.; Beratan, D. N.; Yang, W.; *J. Chem. Theory Comput.* **2011**, *7*, 625. [Crossref]
38. *RheoWin 4.10.0000*, v.2.9; Thermo Fisher Scientific, Germany, 2020.
39. Rasband, W.; *ImageJ*, v. 2.0.0-rc-3; National Institutes of Health, USA, 2014.
40. Albano, J. M. R.; Grillo, D.; Facelli, J. C.; Ferraro, M. B.; Pickholz, M.; *Processes* **2019**, *7*, 606. [Crossref]

41. Nagarkar, R.; Patel, J.; *Acta Sci. Pharm. Sci.* **2019**, *3*, 34. [Link] acessed in November 2024
42. Aslam, M.; Kalyar, M. A.; Raza, Z. A.; *Polym. Sci. Eng.* **2018**, *58*, 2132. [Crossref]
43. Sin, L. T.; Rahman, W. A. W. A.; Rahmat, A. R.; Samad, A. A.; *Polymer* **2010**, *51*, 1206. [Crossref]
44. Zhao, L.; von Hopffgarten, M.; Andrada, D. M.; Frenking, G.; *Wiley Interdiscip Rev.: Comput. Mol. Sci.* **2018**, *8*, e1345. [Crossref]
45. Lu, Q.; Neese, F.; Bistoni, G.; *Phys. Chem. Chem. Phys.* **2019**, *21*, 11569. [Crossref] [PubMed]
46. Yepes, D.; Neese, F.; List, B.; Bistoni, G.; *J. Am. Chem. Soc.* **2020**, *142*, 3613. [Crossref] [PubMed]
47. Kamel, M.; Raissi, H.; Hashemzadeh, H.; Mohammadifard, K.; *Amino Acids* **2020**, *52*, 1465. [Crossref]
48. Sun, Y. P.; Ren, X. H.; Wang, H. J.; Shan, Y. Y.; Xing, L. J.; *Struct. Chem.* **2009**, *20*, 213. [Crossref]
49. Zhao, Z. W.; Dong, Y. J.; Geng, Y.; Li, R. H.; Guan, W.; Su, Z. M.; *J. Org. Chem.* **2021**, *86*, 484. [Crossref]
50. Maity, B.; Scott, T. R.; Stroscio, G. D.; Gagliardi, L.; Cavallo, L.; *ACS Catal.* **2022**, *12*, 13215. [Crossref]
51. Dong, Y. J.; Zhao, Z. W.; Geng, Y.; Su, Z. M.; Zhu, B.; Guan, W.; *Inorg. Chem.* **2023**, *62*, 1156. [Crossref]
52. Li, R. H.; Zhu, B.; Wang, S.; Geng, Y.; Yan, L. K.; Su, Z. M.; Yao, L. S.; Zhong, R. L.; Guan, W.; *Org. Chem. Front.* **2020**, *7*, 2168. [Crossref]
53. Narth, C.; Maroun, Z.; Boto, R. A.; Chaudret, R.; Bonnet, M. L.; Piquemal, J. P.; Contreras-García, J.; In *Applications of Topological Methods in Molecular Chemistry*; Chauvin, R.; Lepetit, C.; Silvi, B.; Alikhani, E., eds.; Springer: Switzerland, 2016, p. 491. [Crossref]
54. Akman, F.; Demirpolat, A.; Kazachenko, A. S.; Kazachenko, A. S.; Issaoui, N.; Al-Dossary, O.; *Molecules* **2023**, *28*, 2684. [Crossref]
55. Zhang, C.; Yuan, X.; Wu, L.; Han, Y.; Sheng, J.; *Eur. Polym. J.* **2005**, *41*, 423. [Crossref]
56. Shi, J.; Yang, E.; *J. Nano Res.* **2015**, *32*, 32. [Crossref]
57. Chhabra, R. P. In *Rheology of Complex Fluids*; Krishnan, J. M.; Deshpande, A. P.; Sunil Kumar, P. B., eds.; Springer: New York, USA, 2010, ch. p. 3. [Link] accessed in November 2024
58. Lenk, R. S. In *Polymer Rheology*; Lenk, R. S., ed.; Springer: Netherlands, 1978, p 1. [Link] accessed in November 2024
59. Briscoe, B.; Luckham, P.; *Polymer* **2000**, *41*, 3851. [Crossref]
60. Das, A.; Uppaluri, R.; Das, C.; *Int. J. Biol. Macromol.* **2020**, *146*, 70. [Crossref]
61. Osswald, T.; Rudolph, N.; Osswald, T.; Rudolph, N.; *Generalized Newtonian Fluid (GNF) Models*; Carl Hanser Verlag GmbH & Co. KG: München, 2015, ch. 3, p. 59-99. [Crossref]
62. Vecchi, C. F.; Cesar, G. B.; de Souza, P. R.; Caetano, W.; Bruschi, M. L.; *Pharm. Dev. Technol.* **2021**, *26*, 138. [Crossref]
63. Chen, D. X. B.; *Extrusion Bioprinting of Scaffolds for Tissue Engineering Applications*; Springer International Publishing: Switzerland, 2018, p. 91. [Link] accessed in November 2024
64. Koski, A.; Yim, K.; Shivkumar, S.; *Mater. Lett.* **2004**, *58*, 493. [Crossref]
65. Yao, L.; Haas, T. W.; Guiseppi-Elie, A.; Bowlin, G. L.; Simpson, D. G.; Wnek, G. E.; *Chem. Mater.* **2003**, *15*, 1860. [Crossref]
66. Kimizuka, N.; *Self-Assembled Nanomaterials I*; Shimizu, T., ed.; Springer: Verlag Berlin Heidelberg, 2008, p. 1. [Crossref]
67. Wang, Y.; Hsieh, Y.-L.; *J. Appl. Polym. Sci.* **2010**, *116*, 3249. [Crossref]
68. Zadeh, M. M. A.; Keyanpour-Rad, M.; Ebadzadeh, T.; *Ceram. Int.* **2014**, *40*, 5461. [Crossref]
69. Mahmud, M. M.; Perveen, A.; Matin, M. A.; Arafat, M. T.; *Mater. Res. Express* **2018**, *5*, 115407. [Crossref]
70. Gupta, D.; Jassal, M.; Agrawal, A. K.; *RSC Adv.* **2016**, *6*, 102947. [Crossref]
71. Park, J.-C.; Ito, T.; Kim, K.-O.; Kim, K.-W.; Kim, B.-S.; Khil, M.-S.; Kim, H.-Y.; Kim, I.-S.; *Polym. J.* **2010**, *42*, 273. [Crossref]
72. Matabola, K. P.; Mokhena, T. C.; Sikhwivhilu, K.; Mokhothu, T. H.; Mochane, M. J.; *Int. J. Environ. Sci. Technol.* **2023**, *20*, 7029. [Crossref]
73. Vu, T. H. N.; Morozkina, S. N.; Sitnikova, V. E.; Nosenko, T. N.; Olekhnovich, R. O.; Uspenskaya, M. V.; *Polym. Bull.* **2024**, *81*, 9669. [Crossref]
74. Kim, K.-J.; Lee, S.-B.; Han, N. W.; *Polym. J.* **1993**, *25*, 1295. [Crossref]
75. Barzegar, F.; Bello, A.; Fabiane, M.; Khamlich, S.; Momodu, D.; Taghizadeh, F.; Dangbegnon, J.; Manyala, N.; *J. Phys. Chem. Solids* **2015**, *77*, 139. [Crossref]
76. Restrepo, I.; Medina, C.; Meruane, V.; Akbari-Fakhrabadi, A.; Flores, P.; Rodríguez-Llamazares, S.; *Polímeros* **2018**, *28*, 169. [Crossref]
77. do Nascimento, F. C.; de Aguiar, L. C. V.; Costa, L. A. T.; Fernandes, M. T.; Marassi, R. J.; Gomes, A. S.; de Castro, J. A.; *Polym. Bull.* **2021**, *78*, 917. [Crossref]

*Submitted: June 30, 2024*
*Published online: November 26, 2024*